http://dx.doi.org/10.5012/bkcs.2013.34.11.3350

The Influence of Collision Energy on the Reaction H+HS→H_2+S

Yanlei Liu, Hongsheng Zhai, Zunlue Zhu, and Yufang Liu*

*Department of Physics, Henan Normal University, Xinxiang 453007, China. *E-mail: yf-liu@henannu.edu.cn*
Received July 15, 2013, Accepted August 26, 2013

Quasi-classical trajectory calculations have been carried out for the reaction H+HS by using the newest triplet $^3A''$ potential energy surface (PES). The effects of the collision energy and reagent initial rotational excitation are studied. The cross sections and thermal rate constants for the title reaction are calculated. The results indicate that the integral cross sections (ICSs) are sensitive to the collision energy and almost independent to the initial rotational states. The ro-vibrational distributions for the product H_2 at different collision energies are presented. The investigations on the vector correlations are also performed. It is found that the collision energies play a postive role on the forward scatter of the product molecules. There is a negative influence on both the alignment and orientation of the product angular momentum for low collision energy at low energy region. Whereas the influence of collision energy is not obvious at high energy region.

Key Words : Quasi-classical trajectory, Integral cross section, Ro-vibrational distribution, Vector correlation

Introduction

The system of S+H_2 has been studied in both theoretical[1-9] and experimental[10,11] methods due to its important role in combustion and atmospheric chemistry. Maiti *et al*.[4] have studied the intersystem crossing effect in the reaction S+H_2 by employing a "mixed" representation approach in conjunction with a trajectory surface-hopping method. They have compared the intersystem crossing effect with that of the reaction O+H_2. Klos *et al*.[6] have reported their theoretical study on the S(^{1}D)+H_2/D_2→SH+H/SD+D reaction, including the nonadiabatic effect. They found that the dependence of the cross-sections upon the product rotational quantum number shows a statistical behavior, which is similar to the result computed with the simple prior statistical model. In the study of Berteloite *et al*.,[7] kinetics and crossed-beam experiments were performed in experimental conditions approaching the cold energy regime. By employing the quantum mechanical (QM) hyperspherical reactive scattering method and quasi-classical trajectory (QCT) and statistical quasi-classical trajectory (SQCT) approaches, Lara *et al*.[8] have calculated the reaction probabilities as a function of total angular momentum (opacity function) and the resulting reaction cross-section for the reaction S+H_2 at low energies (0.09-10 meV) based on two different ab initio potential energy surfaces (PESs). S. H. Lee and Liu[10,11] have investigated the S(^{1}D)+H_2, D_2, and HD reactions through Doppler-selected time-of-flight detection of the H or D product. They have determined the excitation functions and the differential cross-section at several collision energies, as well as the isotopic branching in the S(^{1}D)+HD reaction.

The inverse reaction H+HS has also attracted the attentions. The first global potential energy surface was reported by Martin[12] in 1983 and the reaction H+HS calculation is performed. In 2012, an accurate ab initio potential energy surface (PES) for the lowest triplet state of H_2S was reported by Lv *et al*..[13] The exact quantum dynamical studies on both the abstraction and exchange channels by using this PES have been presented. The results show that there is no well on the H+HS→H_2+S reaction channel (abstraction channel) and the minimum energy paths (MEP) of the abstraction process occur at the collinear configuration. This indicates that the height of the barrier for the abstraction process will increase when the H-H-S bond angles decrease from 180º to 0º. In Ref. 13, the barrier of the reaction H+HS→H_2+S is about 0.09 eV.

The stereo-dynamic studies, providing direct insight into the underlying chemical process based on vector properties, have been performed recently.[14-23] The vector properties such as orientation and alignment of the product molecules for the reaction A+BC→AB+C were investigated in detail, especially by Han *et al*..[18-21, 23] Combined with scalar ones, the vector properties can help to reveal the details of the reaction with rich space information. As mentioned above, most of the investigations on the reaction S+H_2 and its inverse reaction H+HS basically deal with the scalar properties. To our best knowledge, only one study has been reported thus far concerning the stereo-dynamics of the reaction H+HS. Bai *et al*.[24] performed the QCT calculations on both the H+HS→H_2+S and H+SH'→HS+H' reactions. The scalar properties including the reaction probability and integral cross section are calculated in their work, the vector correlations such as ***k-k'***, ***k-j'*** and ***k-k'-j'*** are presented as well.

In this work, we have the further QCT calculations employing the newest potential energy surface (PES) constructed by Lv *et al*..[13] Though the collision energy effect on the stereo-dynamics of the title reaction has been studied by Bai *et al*.,[24] we argue that the reaction is so significant in dynamical features that it merits further study. In this paper, the ro-vibrational distributions at lower collision energies have been obtained, which are entirely different from the

vibrational distributions at higher collision energies. In addition, the opacity function is calculated and the four generalized polarization-dependent differential cross-section (PDDCSs) are discussed in details. This shows that our current study on the stereo-dynamics of the title reaction is of great significance. This work is organized as follows: Section 2 reviews the theoretical methodologies used in the present study. Section 3 presents the calculated results and discussion. The conclusion is presented in Section 4.

Quasi-classical Trajectory Method

The quasi-classical trajectory (QCT) method employed in this study is the same as the method has been used in previous works.[16-18,23] In our calculation, the classical Hamilton's equations are numerically integrated for motion in three dimensions, and the accuracy of the calculation is verified by checking the conservation of both the total energy and angular momentum. The forms of the Hamilton's equations in the QCT method are:

$$\dot{Q}_j = \frac{1}{\mu_{BC}} P_j \quad (j = 1, 2, 3) \tag{1}$$

$$\dot{Q}_j = \frac{1}{\mu_{A-BC}} P_j \quad (j = 4, 5, 6) \tag{2}$$

$$-\dot{P}_j = \left(\frac{\mu_{BC}^2}{m_B^2} \frac{1}{r_{AB}} \frac{\partial U}{\partial r_{AB}} + \frac{1}{r_{BC}} \frac{\partial U}{\partial r_{BC}} + \frac{\mu_{BC}^2}{m_C^2} \frac{1}{r_{AC}} \frac{\partial U}{\partial r_{AC}} \right) Q_j + \left(\frac{\mu_{BC}}{m_B} \frac{1}{r_{AB}} \frac{\partial U}{\partial r_{AB}} - \frac{\mu_{BC}}{m_C} \frac{1}{r_{AC}} \frac{\partial U}{\partial r_{AC}} \right) Q_{j+3} \quad (j = 1, 2, 3) \tag{3}$$

$$-\dot{P}_j = \left(\frac{\mu_{BC}}{m_B} \frac{1}{r_{AB}} \frac{\partial U}{\partial r_{AB}} + \frac{\mu_{BC}}{m_C} \frac{1}{r_{AC}} \frac{\partial U}{\partial r_{AC}} \right) Q_{j-3} + \left(\frac{1}{r_{AB}} \frac{\partial U}{\partial r_{AB}} + \frac{1}{r_{AC}} \frac{\partial U}{\partial r_{AC}} \right) Q_j \quad (j = 4, 5, 6) \tag{4}$$

Where r_{AB}, r_{BC} and r_{Ac} means the internuclear distance of AB, BC and AC. m_A, m_B and m_C indicate the mass of atom A, B and C. μ_{BC} present the reduced mass of atom A and B, $\mu_{A\text{-}BC}$ present the reduced mass of atom A and molecule BC.

In addition, the zero-point energy (ZPE) leakage and tunneling play important roles in some reactions, and they are the most severe shortcomings of QCT simulations. However, when it comes to the reaction H+HS, the quantum effects have little influence on the calculation of the reaction probability.[13] A batch of 100000 trajectories were run for each energy for the title reactions and the integration step size in the trajectories was chosen to be 0.1fs, which guarantees the conservation of the total energy and total angular momentum. The maximum value of the impact parameter, b_{max}, was computed by calculating 100000 trajectories at fixed values of the impact parameter, b, systematically increasing the value of b until no reactive trajectories were obtained. The reaction probability, $P_r = N_r/N_t$, is the ratio of the number of reactive trajectories to the total number of trajectories, while the integrate cross section (ICS) is calculated by $\sigma(E) = 2\pi \sum_0^{b_{max}} \frac{N_R(b)}{N(b)} b\Delta b$, $N(b)$ and $N_R(b)$ being the numbers of total and reactive trajectories in a subdivided interval Δb between 0 and b_{max}, respectively.

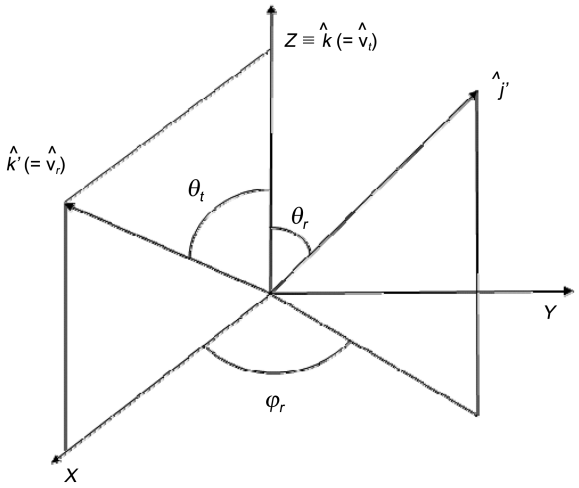

Figure 1. The center-of-mass coordinate system used to describe the ***k***, ***k*** and ***j'*** correlation.

The rate constants can be calculated once the ICSs as a function of collision energy are obtained. Using the state-specific ICSs σ_{vj} for each initial ro-vibrational state of HS and by assuming a Maxwell-Boltzmann distribution over collision energy (E_c), we obtain the specific rate constant k_{vj} at a temperature T given by the standard equation:

$$k_{vj}(T) = (8k_BT/\pi\mu)^{1/2}(k_BT)^{-2} \int_0^{+\infty} \sigma_{vj}(E_c)\exp(-E_c/k_BT)dE_c \tag{5}$$

Where $\sigma_{vj}(E_c)$, is the ICS at E_c (collision energy), μ is the HS-H reduced mass and k_B is the Boltzmann constant.

The center-of-mass (CM) frame[15,17,21] is chosen to describe the vector correlation, and its details are specified as follows. As can be seen in Figure 1, ***k*** is the reactant relative velocity parallel to the z-axis, and ***k*** represents the product relative velocity. The x-z plane, containing vectors ***k*** and ***k***, is the scattering plane. θ_t depicts the angle between ***k*** and ***k***, which indicates the scattering direction of the product. ***j*** is the rotational angular momentum of product, whose polar and azimuthal angles are θ_r and ϕ_r, respectively. $P(\theta_r)$ and $P(\phi_r)$ describe the probability density distribution of reaction products, reflecting ***k-j*** and ***k-k-j*** vector-correlation respectively. The alignment and orientation of ***j*** can be obtained by analyzing $P(\theta_r)$ and $P(\phi_r)$ distributions. Four generalized polarization-dependent differential cross-sections (PDDCSs) are used to describe the full three-dimensional angular distribution associated with ***k-k-j*** correlation in the CM frame. The fully correlated center-of-mass angular distribution is written as[15,18]:

$$P(\omega_t, \omega_r) = \frac{1}{2} \sum_{kq} \frac{[k]}{4\pi\sigma} \frac{d\sigma_{kq}}{d\omega_t} c_{kq}(\theta_r, \phi_r)^* \tag{6}$$

Where $[k] = 2k + 1$, $(1/\sigma)(d\sigma_{kq}/d\omega_t)$ is the generalized polarization-dependent differential cross section (PDDCS) and $c_{kq}(\theta_r, \phi_r)$ are the modified spherical harmonics. The PDDCS is written in the following form:

$$\frac{1}{\sigma}\frac{d\sigma_{kq\pm}}{d\omega_t} = \sum_{k_1}\frac{k_1}{4\pi}S^{k_1}_{kq\pm}C_{k_1q}(\theta_t, 0) \quad (7)$$

where the $S^{k_1}_{kq\pm}$ is evaluated by the expected value expression,

$$S^{k_1}_{kq\pm} = \langle c_{k_1q}(\theta_t, 0)c_{kq}(\theta_t, 0)[(-1)^q e^{iq\phi_r} \pm e^{-iq\phi_r}]\rangle \quad (8)$$

where the angular brackets represent an average over all angles.

The differential cross section is given by

$$\frac{1}{\sigma}\frac{d\sigma_{00}}{d\omega_t} \equiv P(\omega_t) = \sum_{k_1}\frac{k_1}{4\pi}h_0^{k_1}(k_1, 0)P_{k_1}(\cos\theta_t) \quad (9)$$

The function $f(\theta_r)$ can be expanded in a set of Legendre polynomials[15,18]

$$f(\theta_r) = \sum_l a_l p_l(\cos\theta_r) \quad (10)$$

Thus, $l = 2$ indicates the product rotational alignment.

Where, P_2 is a second Legendre moment, and the brackets show an average over the distribution of $\boldsymbol{j'}$ about $\boldsymbol{k}$.

$$\langle P_2(j'\cdot k)\rangle = \frac{1}{2}\langle 3\cos^2\theta - 1\rangle \quad (11)$$

The $P(\theta_r)$ distribution can be expanded in a serious of Legendre polynomials[15,18] as:

$$P(\theta_r) = \frac{1}{2}\sum_k [k]a_0^k P_k(\cos\theta_r) \quad (12)$$

$$a_0^k = \langle P_k(\cos\theta_r)\rangle \quad (13)$$

The expanding coefficient a_0^k are called orientation (k is odd) and alignment (k is even) parameter.

The dihedral angle distribution $P(\phi_r)$ can be expanded in Fourier series[16,20]

$$P(\phi_r) = \frac{1}{2\pi}[1 + \sum_{n\,even\geq 2} a_n\cos n\phi_r + \sum_{n\,odd\geq 1} b_n\sin n\phi_r] \quad (14)$$

$$a_n = 2\langle\cos n\phi_r\rangle \quad b_n = 2\langle\sin n\phi_r\rangle \quad (15)$$

Results and Discussion

Before making further discussion on our calculated results, we compared our QCT reaction probability and ICS for both the abstract reaction and exchange reaction with the QM results.[13] As shown in Figure 2, our QCT results are in good agreement with that the QM result from ref.13. This because the quantum effect is not significant in both the abstract and exchange reactions. What's more, the good agreement between QCT and QM results indicates the accuracy of our calculations and the reliability of our discussion.

To obtain a elementary study on the title reaction, we have calculated the reaction probability as a function of the impact parameter b, which is named the opacity function $P(b)$. Figure 3 depicts the QCT opacity function for the reaction H+HS($v = 0, j = 0$)→H_2+S at four different collision energies. Clearly, the maximum impact parameter b_{max} doesn't change as the collision energy increases. For b less than 1.2 Å, P_r decreases with the increase of the collision energy. At the

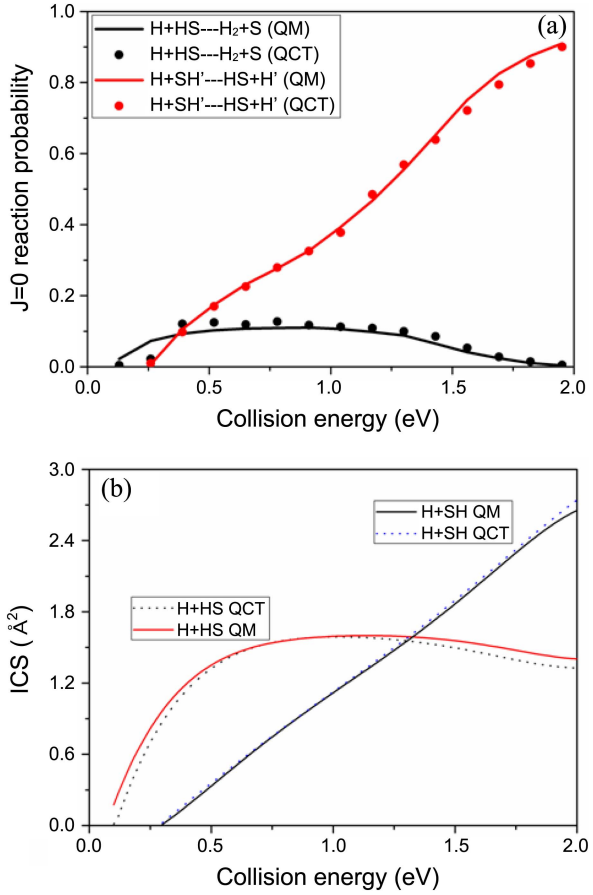

Figure 2. (a) the QCT and QM reaction probabilities for the reactions H+HS and H+SH. (b) the QCT and QM ICSs for the reactions H+HS and H+SH.

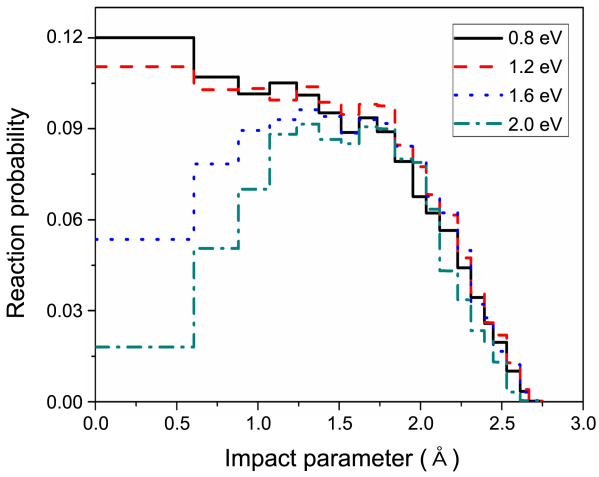

Figure 3. Reaction probability as a function of the impact parameter b at 0.8, 1.2, 1.6 and 2.0 eV for H+HS($v = 0, j = 0$)→H_2+S.

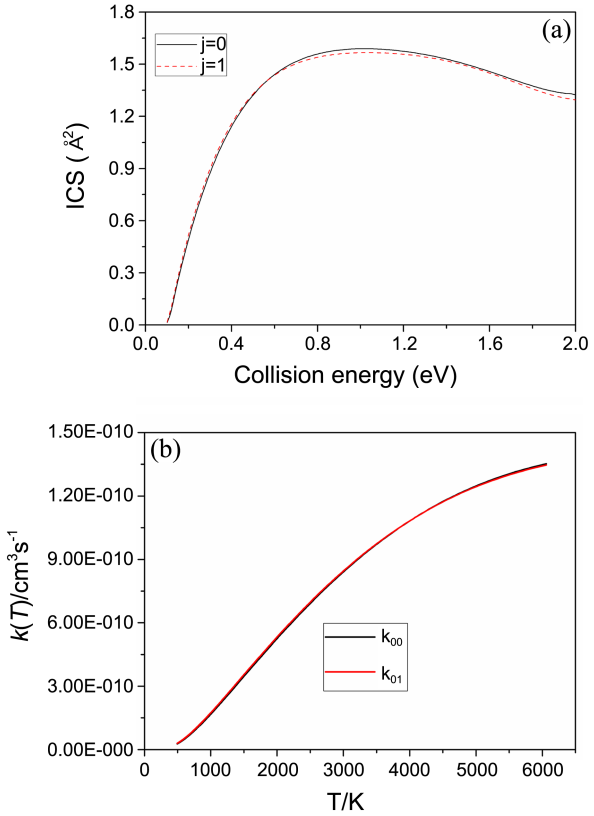

Figure 4. (a) QCT cross section as a function of the collision energy for the reaction H+HS($v = 0$, $j = 0$, 1)→H_2+S (b) QCT rotational state-specific thermal rate constant $k(T)$ for the reaction H+HS($v = 0$, $j = 0$, 1)→H_2+S in the temperature range 500-6000 K.

collision energies of 0.8 and 1.2 eV, the reaction probability tends to decrease as b increases. While, at 1.6 and 2.0 eV, a bell shape is found with peaks located at about $b = 1.2$ Å. It can be concluded that the reactivity with small impact parameter is blocked at high collision energy. This may result from the repulsive potential energy surface (PES). As the collision energy increases, more repulsive regions of the potential energy surface become available and the reactions with small impact parameter are restrained. In addition, the reaction mechanism of the title reaction should be taken in to account.

The QCT ICSs were calculated for different rotational states of reactant HS ($v = 0, j = 0, 1$). Figure 4(a) presents the excitation functions, *i.e.*, ICS as a function of collision energy, for the rotational states $j = 0$ and $j = 1$ of HS. It can be seen clearly, the reaction threshold is 0.09 eV. This result illustrates that the barrier height of the abstraction reaction H+HS→H_2+S is 0.09 eV. The conclusion is accord with that in Ref.13. In Figure 4(a), the curves of the excitation function have the same shape for the different reagent rotation of HS. As the collision energy increases, the integral cross sections reach a high value at 0.8 eV rapidly and then drop slightly after a plateau between 0.8 and 1.2 eV. This tendency is similar with the previous studies for other abstraction reactions H+HBr[25] and H+HCl.[26] The decrease of ICS for the title reaction results from the fact that the total

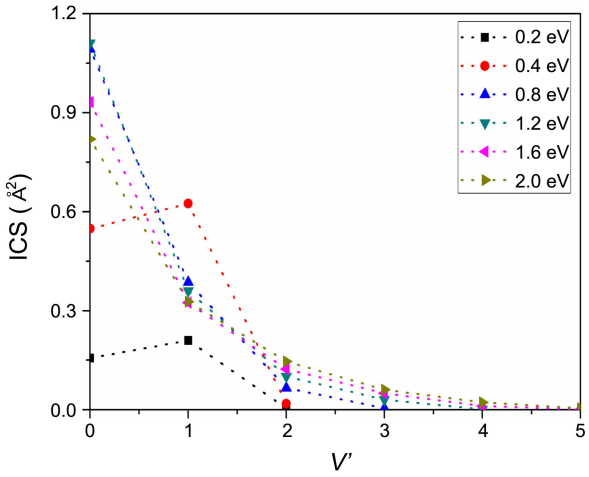

Figure 5. Product vibrational distributions for the reaction H+HS ($v = 0, j = 0$) → H_2+S at 0.2, 0.4, 0.8, 1.2, 1.6 and 2.0 eV.

reaction probability decreases as the collision energy increases. In addition, Figure 4(a) shows that the influence of rotational excitation on HS on ICS is extremely small. Indeed, ICSs change slightly as the rotational quantum number j of HS increases.

Based on the QCT excitation functions, Figure 4(b) shows the thermal rate constants for the rotational states $j = 0, j = 1$ of HS over a wide range of temperatures between 500K and 6000 K. We note that the two thermal rate constants have the same temperature dependence and that the k_{00} and k_{01} increase monotonously as the temperature increases in the range of 500-6000 K. We also found that the effect of the reagent rotational states can be negligible.

To get more insight into the effect of collision energy, the ro-vibrational (v', j') distributions of the product H_2 are calculated in this work. Figure 5 shows the ICSs for the product vibrational distribution at collision energies range from 0.2 to 2.0 eV on the reaction H+HS($v = 0$, $j = 0$)→ H_2+S. We can find that the vibrational excitation of H_2 enhance with the collision energy increasing. As we can see, at the low collision (0.2 and 0.4 eV), the ICSs peaks are found at $v' = 1$ and decrease when the vibrational exited increase. For the high collision energies (0.8, 1.2, 1.6 and 2.0 eV), the most populated vibrational level is $v' = 0$ and ICS regularly decreases with the increase of v'. It can be concluded that the reactions which produce H_2 with high vibrational states are restrained. The vibrational state-resolved ICS at $v' = 0$ decreases distinctly with the increase of collision energy in the range of 1.2-2.0 eV. However, at $v' = 2$, 3 and 4, it shares a slight increment with the collision energy. These reflect the decrease of the total ICS as collision energy increases.

Figure 6 shows the ICSs for ro-vibrational distribution (v' = 0-8, j' = 0-9) of the product H_2 at collision energies range from 0.2 to 2.0 eV on the reaction H+HS(v = 0, j = 0) → H_2+S. It is obvious that the rotational excitation of H_2 enhances as the collision energy increases. In Figure 6, when the collision energy increases, the peaks of the rotational

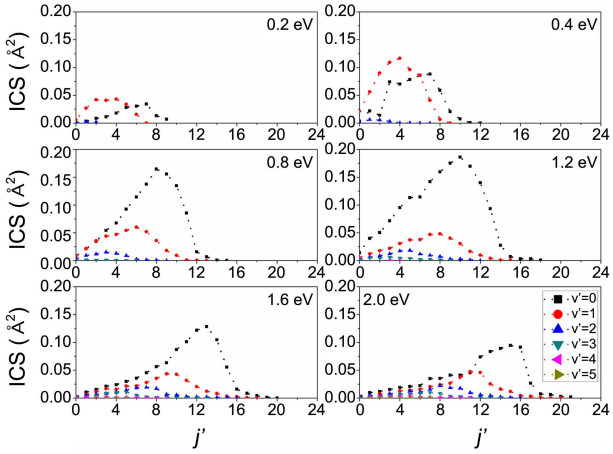

Figure 6. The product rotational distributions on different product vibrational states. Integral cross section at 0.2, 0.4, 0.8, 1.2, 1.6 and 2.0 eV for the H+HS($v = 0, j = 0$)→H_2+S reaction.

excitation shift to the lager rotational quantum number j'. This means that the high rotational excitations become gradually more populated when the collision energy increases. At a given collision energy, the shape of the rotational distributions appears to be distinct for different vibrational levels. The peak of the rotational distributions moves to the smaller j' with increase of v'. At $v' = 0$, for each collision energy, the ICS increases sharply with j', reaches a maximum at a high j' and decreases to negligible values before reaching the last states accessible. However, at the vibrational excited states, bell-shaped curves are visible.

The polarization dependent generalized cross-sections (PDDCSs) depict the ***k-k'-j'*** correlations. Four PDDCSs for the title reaction at collision energies of 0.2, 0.4, 0.8, 1.2, 1.6 and 2.0 eV are shown in Figure 7. The PDDCS $(2\pi/\sigma)(d\sigma_{00}/d\omega_t)$ only describes the scattering directions of the product or the ***k-k'*** correlation. The $(2\pi/\sigma)(d\sigma_{00}/d\omega_t)$ for the reaction H+HS($v = 0, j = 0$)→H_2+S is shown in Figure 6(a). It can be clearly seen that the scattering directions of H_2 are closely related to the collision energy. At lower collision energies of 0.2 and 0.4 eV, the scattering direction of the product H_2 is strongly backward and sideways. As the collision energy increases, the forward scattering strengthen remarkably. The influence of the collision energy on the $(2\pi/\sigma)(d\sigma_{00}/d\omega_t)$ may be attributed to the impulsive effect. With the increase of the collision energy, more repulsive regions of the potential energy surface become available. However, the growth of collision energies con not supplement the more repulsive parts of the surface energetically accessible, which causes an obvious tendency of the forward scattering with the increase of collision energy. The $(2\pi/\sigma)(d\sigma_{20}/d\omega_t)$ is related to the alignment parameter $P_2(j'\cdot k)$, which shows an opposite distribution trend with that of the $(2\pi/\sigma)(d\sigma_{00}/d\omega_t)$ and indicates the alignment of the product angular momentum ***j'*** perpendicular to ***k***. It can be easily seen, in Figure 6(b) that the ***j'*** is preferentially polarized along the direction perpendicular to ***k***. The negative value of the peak of $(2\pi/\sigma)(d\sigma_{20}/d\omega_t)$ becomes smaller with the increment of collision energy in the range of 0.2-0.8 eV, which indicates that the alignment of ***j'*** becomes weaker. When the collision energy increases from 0.8 to 2.0 eV, the alignment of ***j'*** becomes stronger with the negative value of the $(2\pi/\sigma)(d\sigma_{20}/d\omega_t)$ being larger.

At $\theta_t = 0$ and $\theta_t = 180^o$, the PDDCSs $(2\pi/\sigma)(d\sigma_{22+}/d\omega_t)$ and $(2\pi/\sigma)(d\sigma_{21-}/d\omega_t)$ are both nearly zero.[17] Figure 7(c) shows that the values of $(2\pi/\sigma)(d\sigma_{22+}/d\omega_t)$ are almost negative for all scattering angles at the lower collision energies of 0.2 and 0.4 eV, which indicates the notable preference of the alignment along the y-axis. Clearly, the negative value of $(2\pi/\sigma)(d\sigma_{22+}/d\omega_t)$ at 0.4 eV is much smaller than that at 0.2eV, reflecting a weaker alignment of ***j'***. At the higher collision energies of 0.8, 1.2, 1.6 and 2.0 eV, the values of $(2\pi/\sigma)(d\sigma_{22+}/d\omega_t)$ are negative at smaller scattering angles ($0^o < \theta < 70^o$) and are positive at larger scattering angles ($70^o < \theta < 180^o$). As collision energy increases, both the negative values of $(2\pi/\sigma)(d\sigma_{22+}/d\omega_t)$ increase, indicating that the alignment of ***j'*** is stronger. However, the positive values of

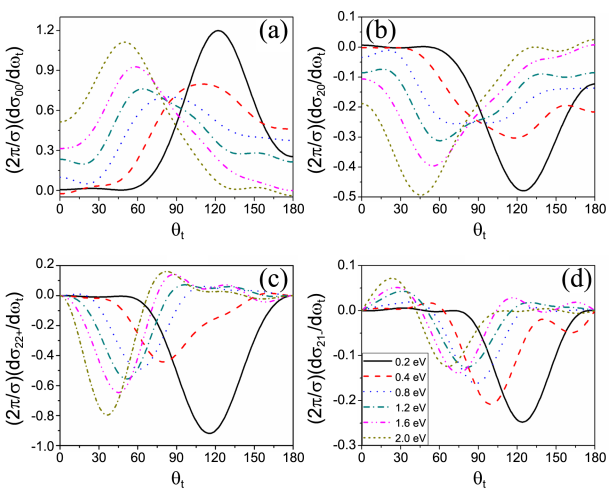

Figure 7. Four PDDCSs for the reaction H+HS($v = 0, j = 0$) →H_2+S at six collision energies.

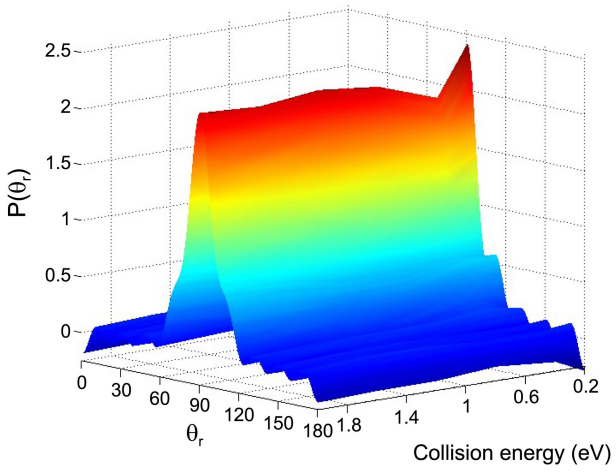

Figure 8. The distribution of $P(\theta_r)$ for the reaction H+HS($v = 0$, $j = 0$)→H_2+S, reflecting ***k-j'*** correlation at six collision energies 0.2, 0.4, 0.8, 1.2, 1.6 and 2.0 eV.

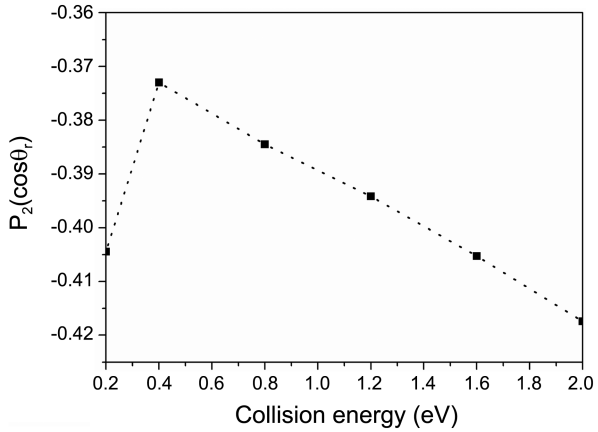

Figure 9. The product rotational alignment parameter $\langle P_2(j'\cdot k)\rangle$ for the reaction H+HS($v = 0$, $j = 0$)→H_2+S as a function of collision energies.

$(2\pi/\sigma)(d\sigma_{22+}/d\omega_t)$ also increase, which may affect the alignment of $\boldsymbol{j'}$. We can conclude that the degree of the alignment of is firstly strongly weakened and then enhanced when the collision energy increases. The $(2\pi/\sigma)(d\sigma_{21-}/d\omega_t)$ is related to the orientation of product rotational angular momentum, which will be discussed later.

Figure 8 shows the $P(\theta_r)$ distributions for the reaction H+HS at six collision energies. In all cases, the symmetric $P(\theta_r)$ distributions exhibit a maximum at $\theta_r = 90^o$, which shows that the product rotational angular momentum vector $\boldsymbol{j'}$ is strongly aligned along the direction perpendicular to the $\boldsymbol{k}$ vector. It is also clear in Fig. 8 that the distribution of $P(\theta_r)$ becomes much weaker when the collision energy increases from 0.2 eV to 0.4 eV, while it becomes stronger when the collision energy increases from 0.4 eV to 1.2 eV. When the collision energy increases from 1.2 eV to 1.6 eV, the alignment of $\boldsymbol{j'}$ becomes weaker again, and it hardly changes when the collision energy is larger than 1.6 eV.

The alignment parameters $\langle P_2(j'\cdot k)\rangle$ are plotted in Figure 9, which give a simple way to express the degree of the product rotational alignment effect. It can be seen from Figure 9 that the $\langle P_2(j'\cdot k)\rangle$ values increase evidently when the collision energy is below 0.4 eV and drops remarkably from 0.4 eV to 2.0 eV. This indicates that the product alignment becomes weaker and then stronger as collision energy increases. This result is distinctly different from that of $P(\theta_r)$. Although the $\langle P_2(j'\cdot k)\rangle$ gives a simple way to express the product alignment, it is not enough to express the degree of the product rotational alignment for the title reaction.

Figure 10 depicts the $P(\phi_r)$ distribution for the reaction H+HS(v = 0, j = 0)→H_2+S at six collision energies 0.2, 0.4, 0.8, 1.2, 1.6 and 2.0 eV. For all the collision energies, the $P(\phi_r)$ distributions are asymmetric with respect to the scattering plane (or about $\phi_r = 180^o$), with a peak appearing at $\phi_r = 270^o$. This means an obvious preference for orientation along the negative y-axis, and implies a preference for the left-hand rotation of the product H_2. As Figure 10 shows, the peak of $P(\phi_r)$ at 0.2 eV is high and narrow, reflecting the strong orientation of the product rotational angular momentum. It can be concluded that the in-plane mechanism dominate the title reaction at lower collision energies. When the collision energy increases in the range of 0.2-0.8 eV, the peak of $P(\phi_r)$ has a sharp decrease, indicating an evident weakness of the orientation. The $P(\phi_r)$ distribution changes slightly when the collision energy increases from 0.8 eV to 2.0 eV, which shows that the energy effect on the product orientation is almost negligible in the region of the higher collision energy.

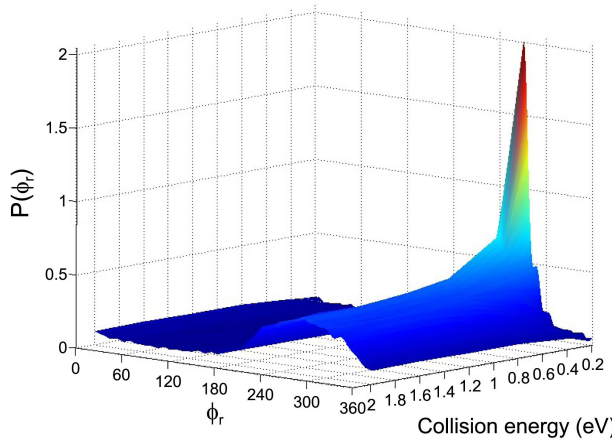

Figure 10. The dihedral angle distribution of $P(\phi_r)$ for the reaction H+HS($v = 0$, $j = 0$)→H_2+S at six collision energies 0.2, 0.4, 0.8, 1.2, 1.6 and 2.0 eV.

Conclusion

To summarize our work, a series of QCT calculations have been performed to investigate the influence of collision energy on the stereo-dynamics. The newest potential energy surface reported by Lv *et al.* is employed in our calculations. It is found that the ICSs increase and then decrease as the collision energy increases. The effect of the initial rotational states on the ICSs and the thermal rate constants is negligible. Both the vibrational and rotational excitation of the products molecule H_2 enhance when the collision energy increases. And the results indicate that the reactions which produce H_2 with high vibrational states are restrained. The rotational distributions are sensitive to both the product vibrational excitation and collision energy. In addition, the vector correlations are computed and discussed. It is concluded that the scattering direction moves forward as the collision energy increases. For lower collision energies, the energy has a negative influence on both the alignment and orientation of the product angular momentum. However, the influence of collision energy is not obvious when the collision energy is higher.

Acknowledgments. This work is supported by the National Natural science Foundation of China (Grant No. 11274096), the Innovation Scientists and Technicians Troop Construction Projects of Henan Province (Grant No. 124200510013) and the Base and Cutting-edge Technology Research Projects of

Henan Province (Grant No. 132300410428). And the publication cost of this paper was supported by the Korean Chemical Society.

References

1. Sengupta, B.; Curtiss, L.; Miller, J. *J. Chem. Phys.* **1996**, *104*, 9888.
2. Shiina, H.; Oya, M.; Yamashita, K.; Miyoshi, A.; Matsui, H. *J. Phys. Chem.* **1996**, *100*, 2136.
3. Shiina, H.; Miyoshi, A.; Matsui, H. *J. Chem. Phys. A* **1998**, *102*, 3556.
4. Maiti, B.; Schatz, G. C.; Lendvay, G. *J. Chem. Phys. A* **2004**, *108*, 8772.
5. Banares, L.; Castillo, J.; Honvault, P.; Launay, J. M. *Phys. Chem. Chem. Phys.* **2005**, *7*, 627.
6. Kłos, J. A.; Dagdigian, P. J.; Alexander, M. H. *J. Chem. Phys.* **2007**, *127*, 154321.
7. Berteloite, C.; Lara, M.; Bergeat, A.; Le Picard, S. D.; Dayou, F.; Hickson, K. M.; Canosa, A.; Naulin, C.; Launay, J. M.; Sims, I. R.; Costes, M. *Phys. Rev. Lett.* **2010**, *105*, 203201.
8. Lara, M.; Dayou, F.; Launay, J. M. Phys. *Chem. Chem. Phys.* **2011**, *13*, 8359.
9. Lara, M.; Jambrina, P.; Varandas, A.; Launay, J. M.; Aoiz, F. *J. Chem. Phys.* **2011**, *135*, 134313.
10. Lee, S. H.; Liu, K. *Chem. Phys. Lett.* **1998**, *290*, 323.
11. Lee, S. H.; Liu, K. *App. Phys B: Lasers and Optics* **2000**, *71*, 627.
12. Martin, R. L. *Chem. Phys.* **1983**, *82*, 337.
13. Lv, S. J.; Zhang, P. Y.; Han, K. L.; He, G. Z. *J. Chem. Phys.* **2012**, *136*, 94308.
14. Karplus, M.; Porter, R.; Sharma, R. *J. Chem. Phys.* **1965**, *43*, 3259.
15. Prisant, M. G.; Rettner, C. T.; Zare, R. N. *J. Chem. Phys.* **1981**, *75*, 2222.
16. Shafer-Ray, N. E.; Orr-Ewing, A. J.; Zare, R. N. *J. Phys. Chem.* **1995**, *99*, *7591.*
17. Aoiz, F.; Brouard, M.; Enriquez, P. J. *Chem. Phys.* **1996**, *105*, 4964.
18. Han, K. L.; He, G. Z.; Lou, N. Q. *J. Chem. Phys.* **1996**, *105*, 8699.
19. Wang, M. L.; Han, K. L.; He, G. Z. *J. Chem. Phys.* **1998**, *109*, 5446 .
20. Wang, M. L.; Han, K. L.; He, G. Z. *J. Chem. Phys. A* **1998**, *102*, 10204.
21. Chen, M. D.; Han, K. L.; Lou, N. Q. *J. Chem. Phys.* **2003**, *118*, 4463.
22. Rassolov, V. A.; Garashchuk, S.; Schatz, G. C. *J. Chem. Phys. A* **2006**, *110*, 5530.
23. Liu, Y. F.; Gao, Y. L.; Shi, D. H.; Sun, J. F. *Chem. Phys.* **2009**, *346*, 46.
24. Bai, M. M.; Ge, M. H.; Yang, H.; Zhu, Y. Jun. *Chin. Phys. B* **2012**, *21*, 123401.
25. Zhang, W.; Cong, S.; Zhang, C.; Xu, X.; Chen, M. *J. Chem. Phys. A* **2009**, *113*, 4192.
26. Chen, M. D.; Han, K. L.; Lou, N. Q. *Chem. Phys.* **2002**, *283*, 463.